Supporting Information

High performance Au/$CH_3NH_3PbI_3$/Cu planar-type self-powered photodetector

Chen Jia[a, b], Hongli Liu[a, b, *], Xiaoyuan Zhang[a, b], Shirong Wang[a, b], Xianggao Li[a, b, *].

[a] Tianjin University, School of Chemical Engineering and Technology, Tianjin 300072, China

[b] Collaborative Innovation Center of Chemical Science and Engineering (Tianjin), Tianjin 300072, China

[*] Corresponding author E-mail: liuhongli@tju.edu.cn (Hongli Liu), lixianggao@tju.edu.cn (Xianggao Li)

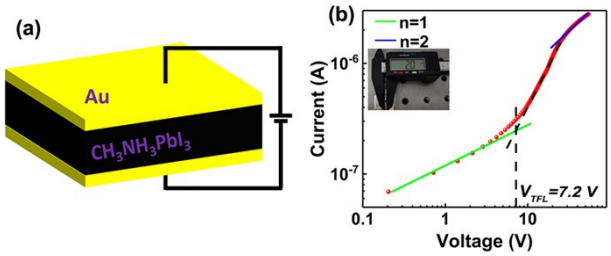

Figure S1. (a) The structure of the hole-only device, (b) the dark *I-V* plot of hole only device, inset: the thickness of $CH_3NH_3PbI_3$ single crystals.

At low electric field, the linear current-voltage (*I-V*) curve (green line) is Ohmic region. When the voltage up to V_{TFL}, the current exhibits a sharp rise, indicating the transition into the trap-filling region, where all trap states are occupied by the injected charge carriers. Trap-filled limit voltage (V_{TFL}) was determined by the defect density using the following equation:

$$V_{TFL} = \frac{en_tL^2}{2\varepsilon\varepsilon_0}$$

where e is the elementary charge, n_t is defect density, ε_0 is the vacuum permittivity and L is the thickness of $CH_3NH_3PbI_3$ single crystals, which is 2 mm (inset of Figure S1b). The relative dielectric constants ε of $CH_3NH_3PbI_3$ is 32. According to the relation between V_{TFL} and the trap density (n_t), the trap density of $CH_3NH_3PbI_3$ single crystal was calculated to be 6.37×10^9 cm^{-3}.

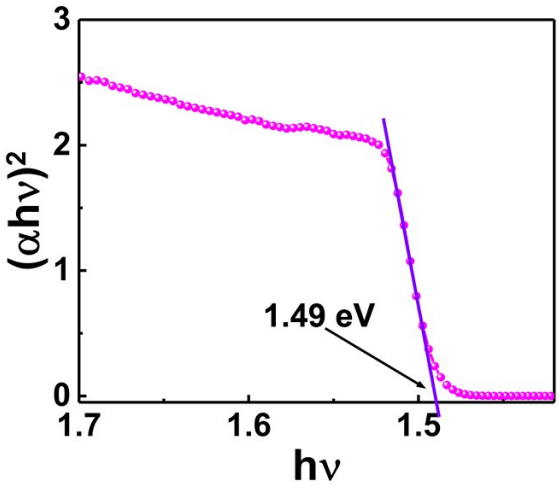

Figure S2. Tauc plot of $CH_3NH_3PbI_3$ single crystals.

The general equation of Tauc plot method is given by: $(\alpha h\nu)^2=K(h\nu-E_g)$. Here α is the absorption coefficient, $h\nu$ is the incident photon energy, K is an energy independent constant, E_g is the bandgap energy. The bandgap of $CH_3NH_3PbI_3$ single crystal is 1.49 eV which can obtain from the Tauc plot as shown in Figure S2.

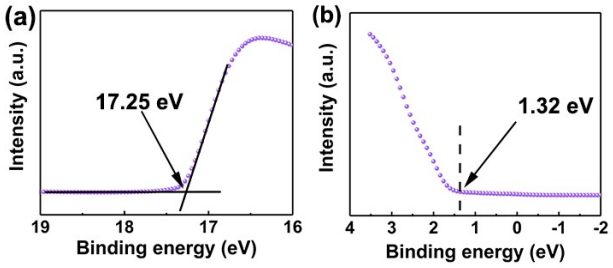

Figure S3. (a) The secondary electron cutoff (SEC) and (b) valance band (VB) edge region of $CH_3NH_3PbI_3$ single crystal via UPS (using He Lyman-α photon source with a photon energy of 21.2eV ($h\nu$).

The valance band (VB) spectra were measured with a monochromatic He I light source (hν=21.2 eV) and a VG Science R4000 analyzer. As ample bias of -5 V was applied to observe the secondary electron cutoff (SEC). The work function can be determined by the difference between the photon energy and the binding energy of the SEC. The work function of perovskite is the difference between the Fermi energy level (E_F) and the vacuum level, which can be obtained from hν-E_2. E_2 can be received from SEC region as shown in Figure S3a, the work function of $CH_3NH_3PbI_3$ single crystal is 3.95 eV. The energy of valance band maximum (E_{VBM}) for perovskite

can be calculated through formula as $E_{VBM}=E_F-E_1$, where E_1 is obtained from VB edge region as Figure S3b. The valance band maximum (VBM) was -5.27 eV.

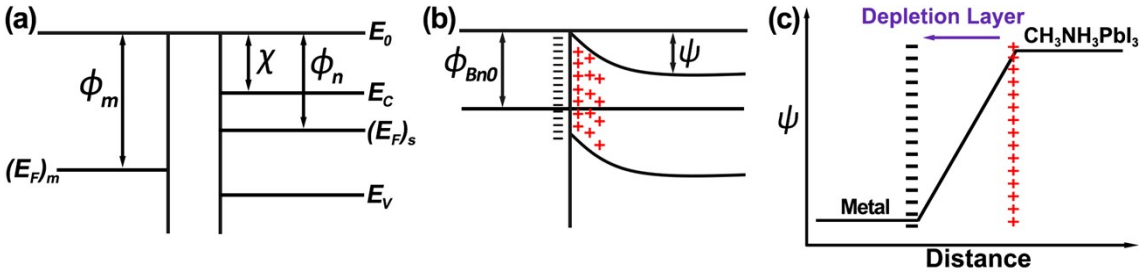

Figure S4. (a) Energy level of metal and semiconductor, (b) depletion layer and Schottky barrier after the metal contacts with semiconductor, (c) contact potential (ψ) caused by the depletion layer.

Here, ϕ_m is the work function of Au (5.1 eV) and Cu (4.65 eV), ϕ_n is the work function of $CH_3NH_3PbI_3$ (3.95 eV). χ is electronic affinity of $CH_3NH_3PbI_3$, ϕ_{Bn0} is Schottky barrier, ψ is contact potential. Figure S4a is the energy level distribution before the metal contacts with the semiconductor, $\phi_m > \phi_n$. Figure S4b shows the electrons in the semiconductor flow to the metal as they contact together, the metal surface is negatively charged due to the inflow of electrons, while the semiconductor is positively charged due to the outflow of electrons. And then depletion layer and Schottky barrier is formed at the contact interface between metal and semiconductor. Figure S4c is the contact potential (ψ) caused by the depletion layer. The depletion layer generates ψ pointing to the surface of metal.

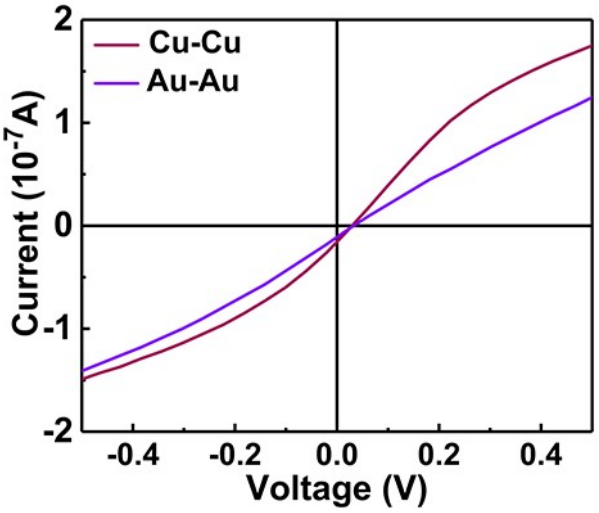

Figure S5. *I-V* curves of the self-powered PDs with symmetrical electrodes.

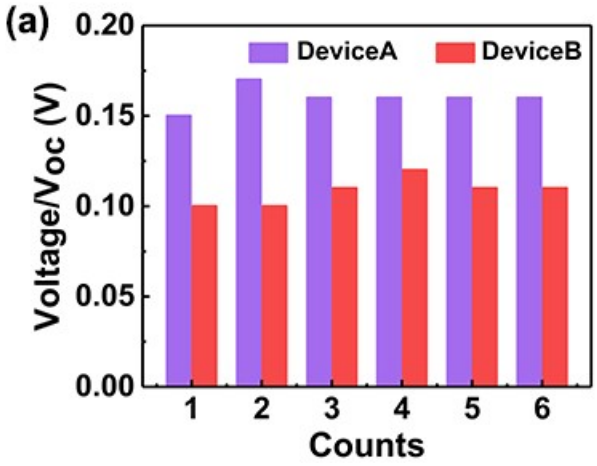

(b)

Device \ Voltage/V	Device A	Device B
1	0.15	0.10
2	0.16	0.11
3	0.17	0.10
4	0.16	0.12
5	0.16	0.11
6	0.16	0.11
Average	0.16	0.11

Figure S6. (a) Cartogram, (b) Statistical table of the driving force of 6 groups Au/$CH_3NH_3PbI_3$/Cu self-powered PDs.

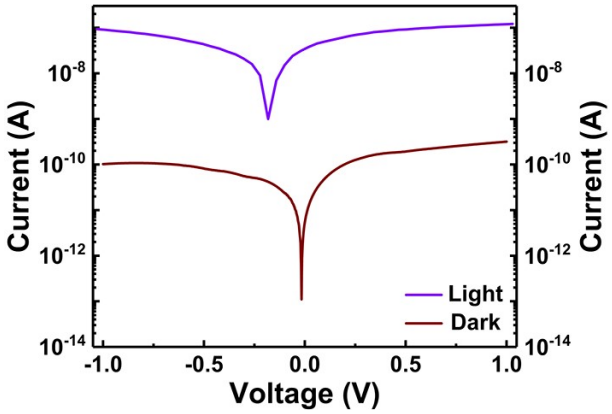

Figure S7. *I-V* curve of Au/$CH_3NH_3PbI_3$/Cu PDs in dark and under illumination.

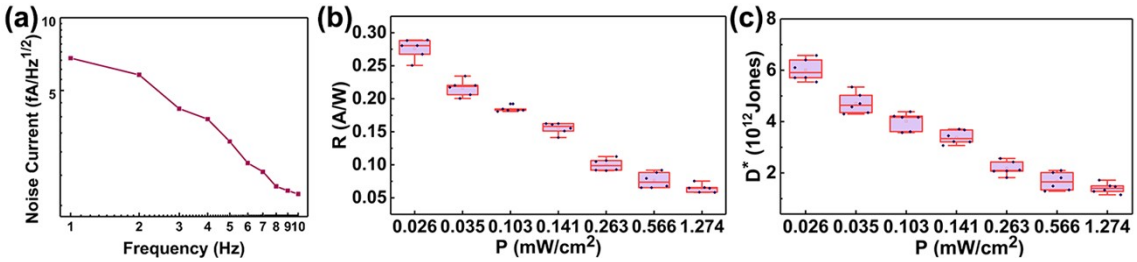

Figure S8. (a) The noise spectra of the device at 0 V bias, (b) responsivity (R) and (c) detectivity (D*) of different batches of devices at various light intensities.

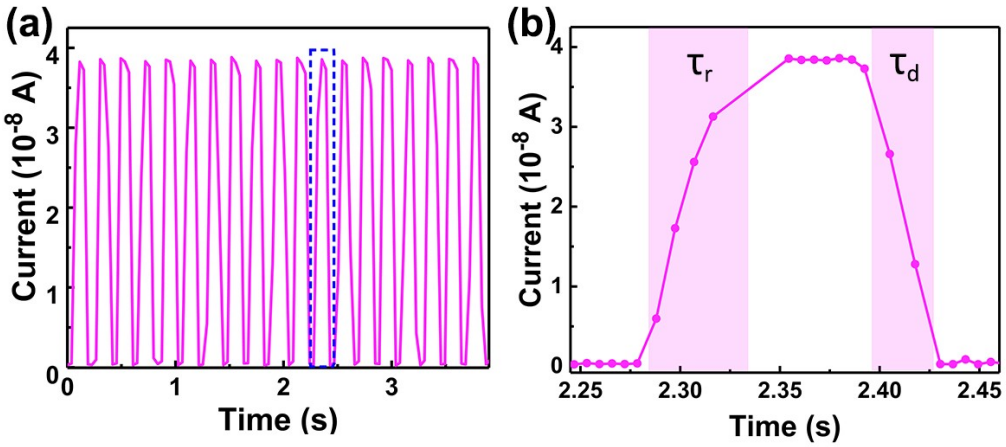

Figure S9. Response time of Au/$CH_3NH_3PbI_3$/Cu PDs.

Table S1. Key performance figure-of-merits of lateral metal-semiconductor-metal (MSM) self-powered photodetectors in our work and other perovskite photodetectors in literatures.

Photodetector structure	Wavelength (nm)	R(A/W)	D*(Jones)	
In/Te/$CsPbBr_3$/In	300-600	3.5×10^{-4}	1.42×10^{10}	[1]
Au/$Cs_2AgBiBr_6$ SC/Ag	365-650	0.16	3.5×10^{10}	[2]
Au/ $MAPbI_3$ SC/Au	400-810	0.16	7.34×10^{11}	[3]
Ni/$CH_3NH_3I_3$ NW/Al	405-808	0.227	1.36×10^{11}	[4]
Au/$CH_3NH_3PbI_3$ MWs/Ag	400-800	0.161	1.3×10^{12}	[5]
Au/$CH_3NH_3PbI_3$ SC/Al	375-830	0.24	/	[6]
Ag/Bi/2D PMA_2PbCl_4 MMB/Bi/Ag	240-800	9	1.01×10^{11}	[7]
Au/ $CH_3NH_3PbI_3$ SC/Cu	400-840	0.288	4.69×10^{12}	This work

Responsivity (R) is defined as follows:

$$R = \frac{I_{light} - I_{dark}}{PS} \quad \text{(Formula S1)}$$

where I_{light} is the photocurrent, I_{dark} is the dark current, P is the illumination power density, and S is the effective illuminated area.

The detectivity (D*) is related to the effective area (A) of the device and the test bandwidth (Δf).

$$D^* = \frac{R\sqrt{A\Delta f}}{I_{noise}} \quad \text{(Formula S2)}$$

Where A is the effective area of the device, Δf is the test bandwidth, and I_{noise} is

the noise current of the devices. The device performance is measured at test bandwidth of 5 Hz.

References

1. J. Zhang and J. Liu, *RSC Adv*, 2022, **12**, 2729-2735.
2. D. Hao, D. Liu, S. Zhang, L. Li, B. Yang and J. Huang, *Adv Opt Mater*, 2022, **10**, 2100786.
3. X. Zhang, X. Dong, S. Wang, H. Liu, W. Hu and X. Li, *Chem. Eng. J.*, 2021, **404**, 125957.
4. J. Tao, Z. Xiao, J. Wang, C. Li, X. Sun, F. Li, X. Zou, G. Liao and Z. Zou, *J. Alloys Compd.*, 2020, **845**, 155311.
5. C.-Y. Wu, W. Peng, T. Fang, B. Wang, C. Xie, L. Wang, W.-H. Yang and L.-B. Luo, *Adv Electron Mater*, 2019, **5**, 1900135.
6. J. Ding, H. Fang, Z. Lian, J. Li, Q. Lv, L. Wang, J.-L. Sun and Q. Yan, *CrystEngComm*, 2016, **18**, 4405-4411.
7. L. Guo, X. Liu, L. Gao, X. Wang, L. Zhao, W. Zhang, S. Wang, C. Pan and Z. Yang, *ACS Nano*, 2022, **16**, 1280-1290.